AD-A154 942 THE PLASMA EROSION OPENING SWITCH(U) NAVAL RESEARCH LAB 1/1
WASHINGTON DC R J COMMISSO ET AL. 14 MAY 85
NRL-MR-5560

UNCLASSIFIED F/G 9/1 NL

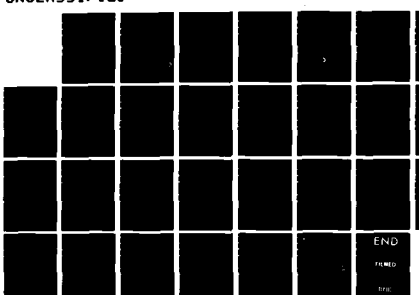

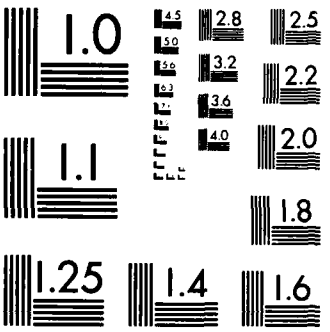

NRL Memorandum Report 5560

The Plasma Erosion Opening Switch

R. J. COMMISSO, G. COOPERSTEIN, R. A. MEGER, J. M. NERI,
P. F. OTTINGER AND B. V. WEBER*

Plasma Technology Branch
Plasma Physics Division

**JAYCOR, Inc.*
Alexandria, VA 22304

May 14, 1985

This research was supported by the Defense Nuclear Agency under Subtask T99QMXLA, work unit 00038 and work unit title "Advanced Simulation Concepts."

NAVAL RESEARCH LABORATORY
Washington, D.C.

SECURITY CLASSIFICATION OF THIS PAGE

REPORT DOCUMENTATION PAGE

1a REPORT SECURITY CLASSIFICATION UNCLASSIFIED	1b RESTRICTIVE MARKINGS
2a SECURITY CLASSIFICATION AUTHORITY	3 DISTRIBUTION/AVAILABILITY OF REPORT Approved for public release; distribution unlimited.
2b DECLASSIFICATION/DOWNGRADING SCHEDULE	
4 PERFORMING ORGANIZATION REPORT NUMBER(S) NRL Memorandum Report 5560	5 MONITORING ORGANIZATION REPORT NUMBER(S)
6a NAME OF PERFORMING ORGANIZATION Naval Research Laboratory 6b OFFICE SYMBOL (If applicable) Code 4770	7a NAME OF MONITORING ORGANIZATION
6c ADDRESS (City, State, and ZIP Code) Washington, DC 20375-5000	7b ADDRESS (City, State, and ZIP Code)
8a NAME OF FUNDING/SPONSORING ORGANIZATION DNA and DOE 8b OFFICE SYMBOL (If applicable)	9 PROCUREMENT INSTRUMENT IDENTIFICATION NUMBER
8c ADDRESS (City, State, and ZIP Code) Washington, DC 20305 Washington, DC 20545	10 SOURCE OF FUNDING NUMBERS PROGRAM ELEMENT NO. (See page ii) / PROJECT NO / TASK NO. / WORK UNIT ACCESSION NO

11 TITLE (Include Security Classification)
The Plasma Erosion Opening Switch

12 PERSONAL AUTHOR(S)
Commisso, R.J., Cooperstein, G., Meger, R.A., Neri, J.M., Ottinger, P.F. and Weber, B.V.*

13a TYPE OF REPORT	13b TIME COVERED	14 DATE OF REPORT (Year, Month, Day)	15 PAGE COUNT
Interim	FROM _____ TO _____	1985 May 14	46

16 SUPPLEMENTARY NOTATION
*JAYCOR, Inc., Alexandria, VA 22304 (Continues)

17 COSATI CODES		
FIELD	GROUP	SUB-GROUP

18 SUBJECT TERMS (Continue on reverse if necessary and identify by block number)
Plasma switches, Inductive store, Opening switch, Pulsed power.

19 ABSTRACT (Continue on reverse if necessary and identify by block number)

The Plasma Erosion Opening Switch (PEOS) can conduct high current (~MA), open quickly (<10ns), and withstand high voltage (~MV). This switching technique has been used in inductive energy storage experiments and can be used with existing generators for pulse compression, voltage multiplication and power multiplication. The PEOS is used routinely for other types of power conditioning including prepulse suppression, pulse sharpening and multimodule jitter reduction. This paper is a review of the PEOS work to date. It reviews basic physics principles of the PEOS and outlines the operational limits of a system that employs a PEOS. Examples of present applications of the PEOS are also discussed.

20 DISTRIBUTION/AVAILABILITY OF ABSTRACT	21 ABSTRACT SECURITY CLASSIFICATION
☒ UNCLASSIFIED/UNLIMITED ☐ SAME AS RPT ☐ DTIC USERS	UNCLASSIFIED
22a NAME OF RESPONSIBLE INDIVIDUAL R. J. Commisso	22b TELEPHONE (Include Area Code) (202) 767-2468 / 22c OFFICE SYMBOL Code 4770

DD FORM 1473, 84 MAR 83 APR edition may be used until exhausted
All other editions are obsolete

SECURITY CLASSIFICATION OF THIS PAGE

10. SOURCE OF FUNDING NUMBERS

PROGRAM ELEMENT NO.	PROJECT NO.	TASK NO.	WORK UNIT ACCESSION NO.
62715H	DE-AI08-79DP40092		DN320-094
DOE		23	DN680-382

16. SUPPLEMENTARY NOTATION (Continued)

To appear as a chapter in a volume on opening switches in a series of books entitled, "Advances in Pulsed Power Technology," edited by M. Kristiansen and A. Guenther.

This research was supported by the Defense Nuclear Agency under Subtask T99QMXLA, work unit 00038 and work unit title "Advanced Simulation Concepts,"

CONTENTS

THE PLASMA EROSION OPENING SWITCH

I. Introduction

Inductive energy storage in conjunction with opening switch techniques has advantages over conventional, capacitive power conditioning for high-energy (>10 MJ), high-power ($>10^{12}$W) applications.[1] The principal advantage of inductive storage derives from the 10-100 times higher energy density possible with energy stored in magnetic fields compared with electric fields and the fact that the energy can be stored at low voltage. In theory, this makes compact and economical generators possible.[2] In any inductive storage scheme, the opening switches represent the most critical elements. One such switch is the plasma erosion opening switch (PEOS). This switch has been proposed to be used either by itself[3] or in sequence with other opening switches[4] in inductive-store pulsed-power systems. Recently, inductive-store/pulse-compression techniques employing the PEOS have been successfully adapted to conventional pulsed-power generators for the purpose of improving their performance, e.g., peak voltage, peak power, pulse width.[5-11] In addition to inductive store applications, the PEOS has been used extensively in high power generators for prepulse suppression, improving power flow symmetry, and current risetime sharpening.[5,6,12-18] Depending on the specific application, the PEOS has demonstrated opening times less than 10 ns, conduction times approaching 100 ns, conduction currents as high as 5 MA, and voltage generation over 3 MV without breakdown. Present research is directed toward obtaining a better understanding of PEOS physics and the interaction of the PEOS with the other system components to optimize system performance.

Manuscript approved March 1, 1985.

*JAYCOR, Inc., Alexandria, Va.

A typical PEOS system is sketched in Fig. 1. Here, the driver may be a conventional pulsed-power generator, a slow capacitor bank (or homopolar generator) with one or more stages of pulse compression prior to the PEOS, or any other appropriate source of current. The PEOS utilizes a source (or sources) of plasma[19,20] located in vacuum between the driver and load. The geometry is such that the plasma is injected between the electrodes so that the plasma is electrically in parallel with the load. The fact that the switch is in vacuum, physically close to the load, helps to minimize the inductance between the load and the switch. Under proper conditions the plasma can conduct the generator pulse to a specified current level, energizing the storage inductance and isolating the load [Fig. 1(a)]. When this current level is reached the switch opens [Fig. 1(b) and (c)] and the generator current is diverted to the load in a time that is short compared with the conduction time. The efficiency of current transfer depends strongly on how well the switch plasma parameters are matched to the system parameters (current, switch area, distribution of inductances, etc.).

Physics understanding of the PEOS has evolved over the years as a result of close interplay between theory and experiment. In this article, we first present important aspects of the switch operation from a phenomenological point of view, so that the reader can obtain a sense of the relevant parameter regimes and switch operational characteristics (Sec. II). This discussion is immediately followed by a description of the switch physics in Sec. III. Using this PEOS physics we outline generic PEOS system performance limits. We review examples of present and future applications of the PEOS in Sec. IV. To provide a consistent and convenient data base, we use the results obtained from the Gamble I generator[21] at the Naval Research Laboratory (NRL).

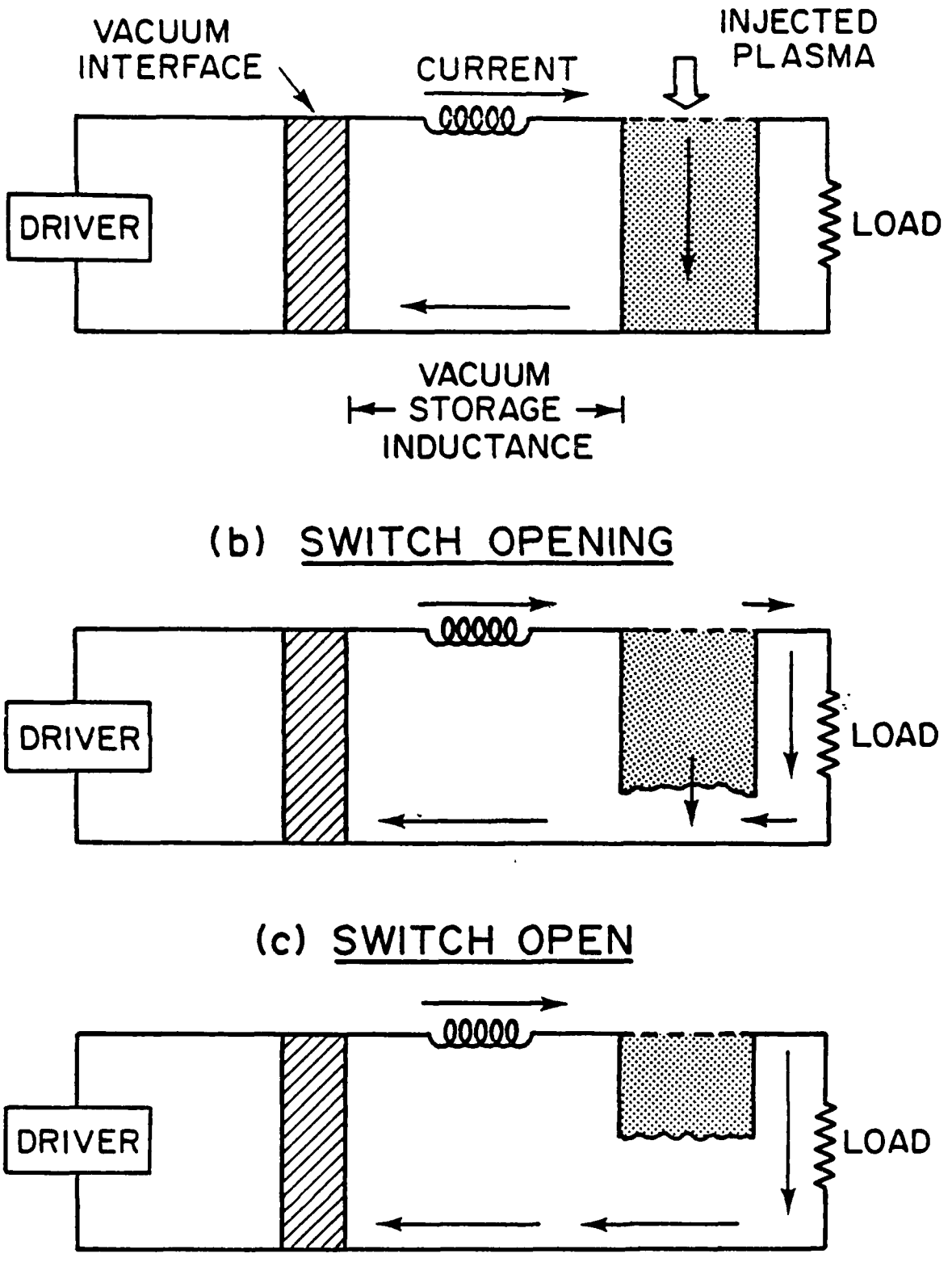

Fig. 1 — Schematic representation of PEOS operation

II. PEOS Phenomenology

The general operation of the PEOS can be described with the aid of Fig. 2(a), which is a schematic of the front end of the Gamble I generator configured for inductive-store/pulse-compression experiments with a PEOS.[10] Also shown are a more detailed view of the switch region [Fig. 2(b)] and a typical generator voltage waveform [Fig. 2(c)] measured at the vacuum insulator with an open circuit load. In Fig. 2(a), Gamble I is shown with an electron-beam (e-beam) diode load while in Fig. 2(b) the e-beam diode is replaced with a short circuit. Plasma is injected toward the cathode (inner conductor) through a screen anode. The plasma source consists of three carbon plasma guns[20] equally spaced in azimuth around the inner conductor. The generator is fired a time interval $_D$ after firing the guns. Negative voltage is applied to the center conductor and current flows through the plasma, energizing the coaxial storage inductance. For the proper combination of plasma parameters the behavior illustrated in Fig. 3 is obtained for a short-circuit load. At some time during the pulse, the generator current I_G (measured by Rogowski loop #1) is rapidly diverted (10 ns opening time) to the load, as evidenced by the time history of the load current I_L (measured by Rogowski loop #2). An equivalent circuit for this arrangement is shown in Fig. 4. Here Gamble I (the driver of Fig. 1) is modeled by a voltage source, V_G [Fig. 2(c) for Gamble I], in series with a generator resistance, R_G (2 for Gamble I). The PEOS is represented by a variable resistance R_S. The transition inductance L_T is the small ($<<L_0$), parasitic inductance associated with the region between the switch and load and R_L is the load resistance (R_L = 0 for a short circuit).

For a given generator pulse and load, the switch behavior can change quite markedly by varying the plasma-gun to electrode separation, the time

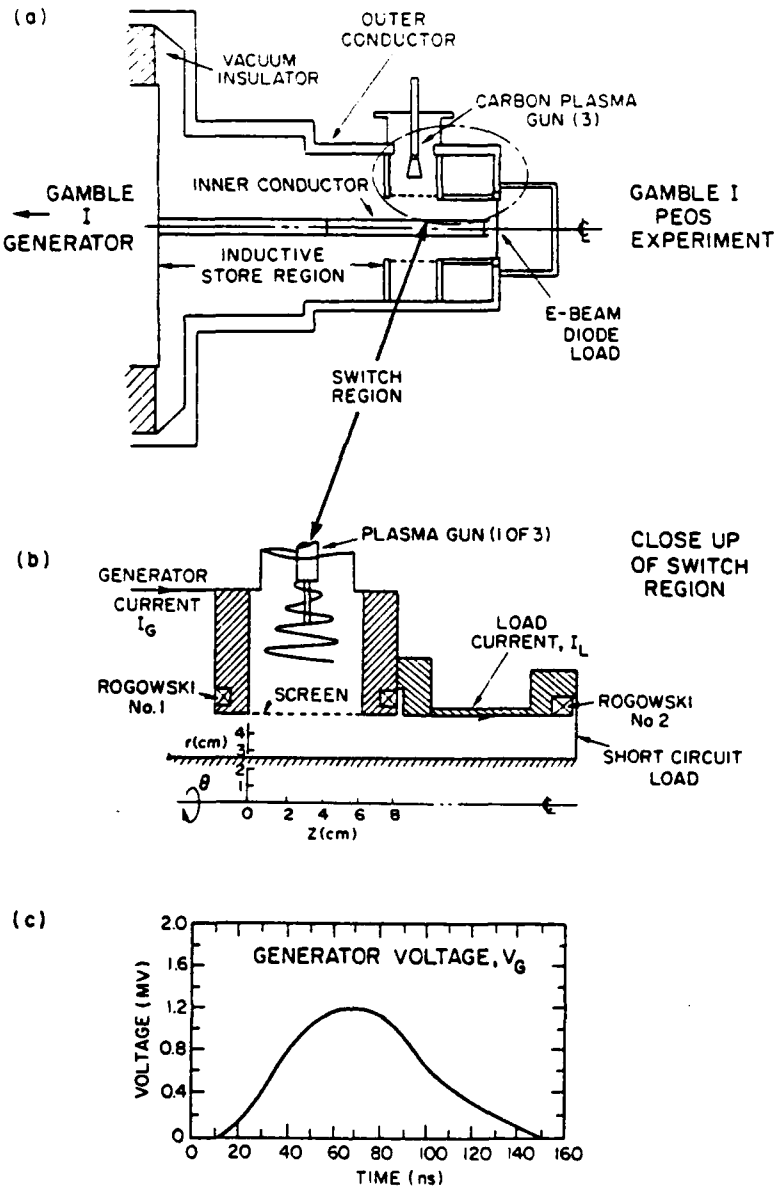

Fig. 2(a) — Schematic of Gamble I PEOS experiment showing relative location of generator, storage inductance, PEOS region, and load. (b) Close up of switch region showing current diagnostics, electrode polarity, and plasma gun orientation. Here the load is a short circuit. (c) Typical Gamble I generator voltage waveform.

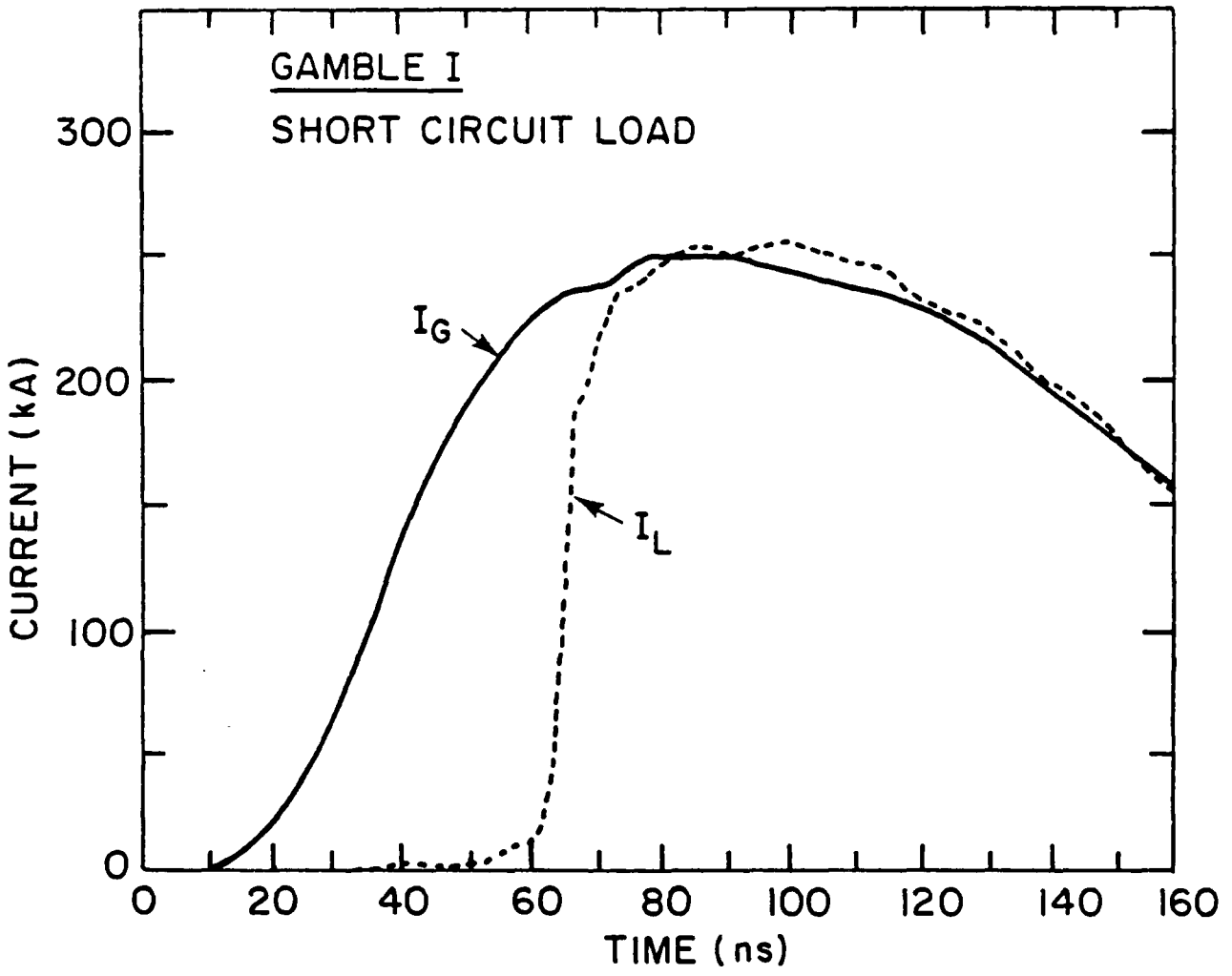

Fig. 3 — Measured currents flowing through the generator (I_G) and load (I_L) for Gamble I with a short circuit load

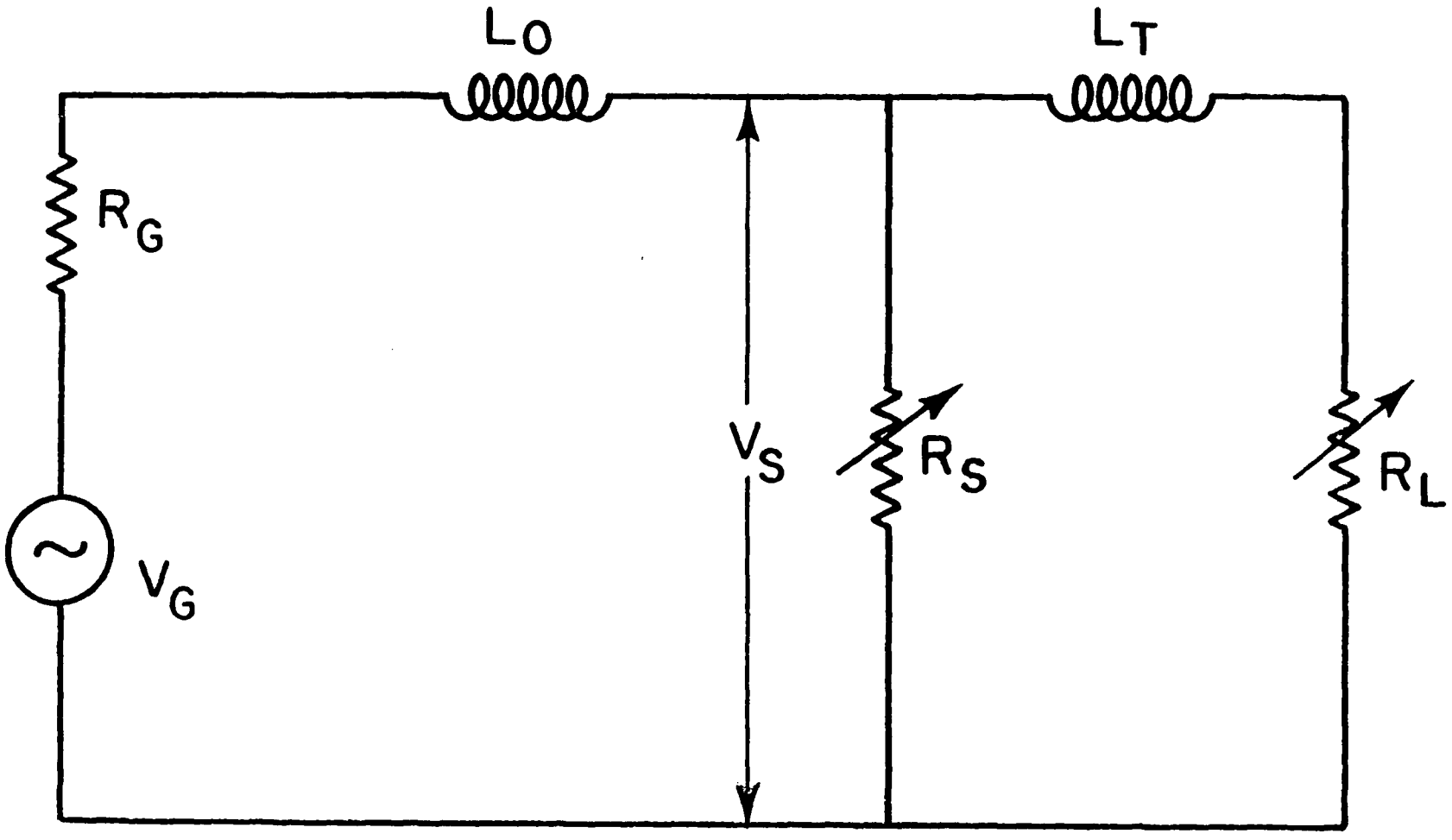

Fig. 4 — Generic equivalent circuit for the application of inductive-store/pulse-compression techniques to conventional generators

interval τ_D [22] and the direction of plasma injection with respect to the polarity of the electrodes.[23] All of these factors affect the relevant PEOS plasma parameters at the time the generator is fired.[24,25] With the configuration illustrated in Fig. 2(b), the fastest openings at the highest currents for the Gamble I parameters occur when τ_D is such that the plasma injection speed is $\gtrsim$ 7 cm/μs, and the switch plasma electron density r is $n_e \approx 3\times10^{13}cm^{-3}$. Here, the plasma is predominantly C^{++} and the electron temperature is $T_e \approx 5eV$. At larger τ_D, n_e increases to $\gtrsim 5\times10^{14}cm^{-3}$, the plasma no longer has large drift speed toward the cathode, and C^+, neutral carbon, and hydrogen have slowly diffused into the switch region from the walls. Under these conditions the PEOS is observed to conduct longer, but the opening is much slower. For large-enough τ_D, the PEOS conducts the entire Gamble I current pulse and never opens. An illustration of this behavior appears in Fig. 5, which is a plot of I_L as a function of time for various values of τ_D obtained from Gamble I with $R_L = 0$ [Fig. 2(b)].

The importance of controlling the direction of plasma injection has been demonstrated by varying the polarity of the electrodes and the injection geometry.[23] Data taken with Gamble I configured as in Fig. 2(b) along with illustrations of the specific plasma injection geometry and electrode polarity are shown in Fig. 6. The data represent optimized opening switch performance. The PEOS behavior is severely degraded for inward radial injection toward the anode [Fig. 6(b)] compared with the case of inward radial injection toward the cathode [Fig. 6(a)]. Using a flashboard source, outward radial injection toward the cathode was achieved. This recovers the fast opening behavior of Fig. 6(a), as illustrated in Fig. 6(c).

Much useful information concerning the switch operation can be conveniently obtained using $R_L = 0$; however, most applications of interest

$$I_i = Zen_i A\left(v_d + \frac{dD}{dt}\right) \tag{6}$$

and I_i is given by Eq. (3). As the gap increases in response to the increasing electron current the voltage across the gap (switch) also increases (because of the Child-Langmuir law) as $V_S^{3/2} \propto D^2 I_S$. If this voltage drives current through the load, we may say that the switch begins to open [Fig. 10(a)].

Until this point the effects of the magnetic field associated with I_S have been ignored. These effects become important when the typical electron Larmor radius becomes comparable to the gap size. For cylindrical geometry, particle-in-cell (PIC) code simulations show that magnetic field effects become important when I_S reaches a critical value given by[35]

$$I_S \gtrsim I_C \equiv 1.36\times10^4(\gamma^2-1)^{1/2}\frac{r_c}{D}, \tag{7}$$

where I_C is in amperes and γ is the ratio of the electron energy to its rest energy. (The PIC code results differ only slightly from simple analytic estimates.)

When I_S approaches I_C of Eq. (7), the electron flow across the gap changes and the electron space-charge distribution in the gap is altered. Electrons now $\vec{E}\times\vec{B}$ drift along the switch length in the self-consistent electric and magnetic fields in the gap, traveling a distance characterized by the length of the switch, $\sim\ell$, rather than just crossing the gap, D, before reaching the plasma. An important consequence associated with this alteration of the electron space charge is a modification of the bipolar space-charge-limited flow condition. The electron space charge near the plasma surface is

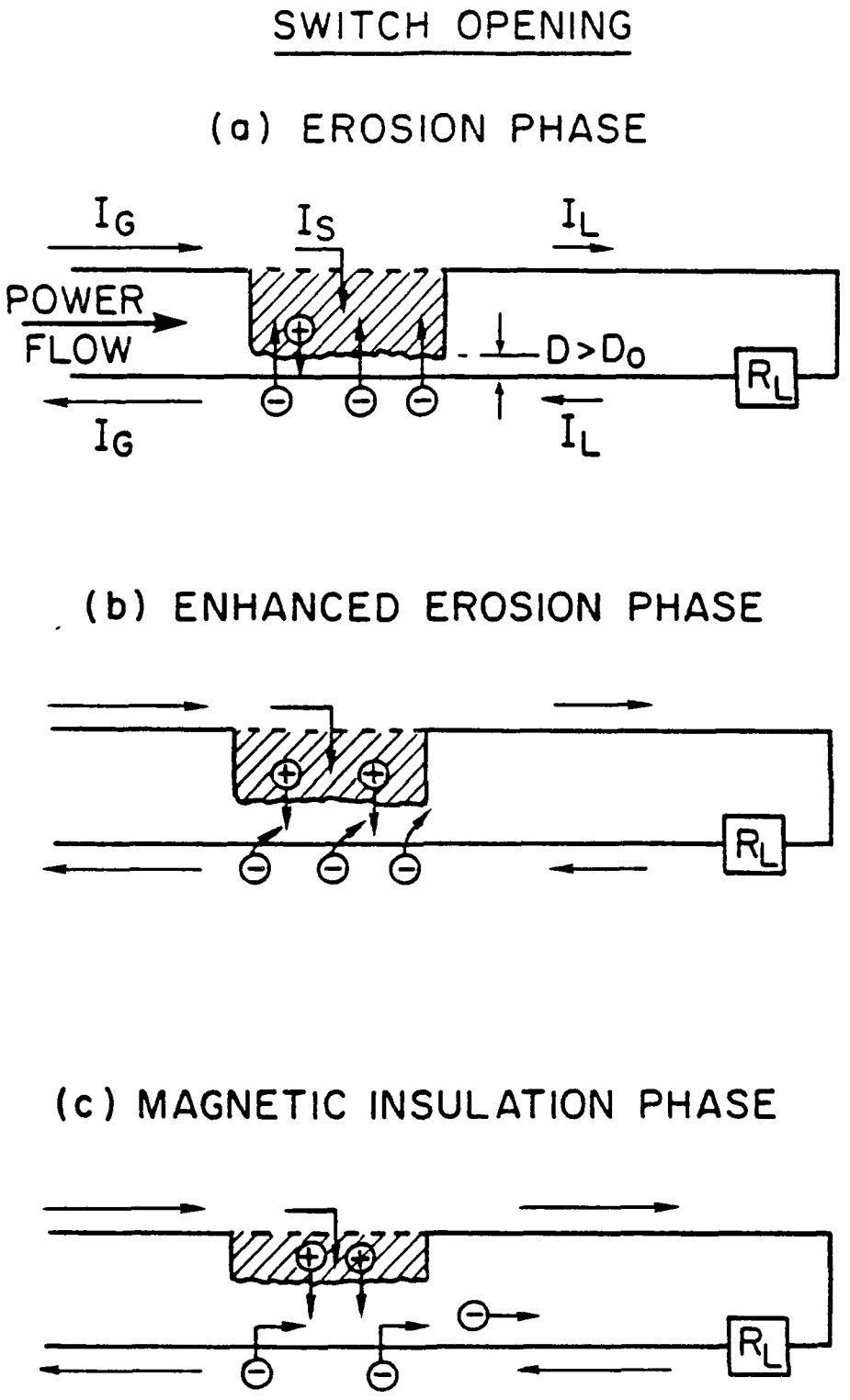

Fig. 10 — Schematic of switch opening: (a) erosion phase, (b) enhanced erosion phase, and (c) magnetic insulation phase.

other processes that provide additional ion flux become dominant, e.g., as a result of plasma-wall interaction or arc phenomena, control of not only conduction but also the rapid opening may be lost. Fortunately, these processes usually take a long time (compared with the timescale for switch operation) to manifest themselves. Control of Γ_i is achieved for the carbon plasma guns discussed previously by varying τ_D, as suggested in Sec. II (Fig. 5). In Fig. 9 a more quantitative demonstration of this control is displayed.[22] Using Gamble I configured as in Fig. 2(b), the maximum switch current I_S^o ($I_S \equiv I_G - I_L$) was measured as a function of τ_D. The ion density and drift velocity at different τ_D were estimated from double floating probes and Faraday cups and used in a circuit interactive computer code that models the entire switch operation.[28] The final current channel width, ℓ, was estimated from the magnetic field measurements.[32] The model, which incorporates the current limit of Eq.(5), and experimental results agree.

2. Switch Opening

The switch opening can be described in three phases: erosion, enhanced erosion and magnetic insulation. These three phases are schematically depicted in Fig. 10. When the current limit of Eq. (5) is reached the plasma must respond in such a way that space charge condition of Eq. (3) remains satisfied. This is accomplished by the gap size increasing.[18,27,33,34] That is, the boundary between the plasma and the non-neutral gap recedes from the cathode, exposing new ions. This process is termed "erosion" and it increases the rate at which ions enter the gap. In the frame of the plasma boundary, the ions acquire an additional drift speed equal to dD/dt, where D(t) is the gap size determined by

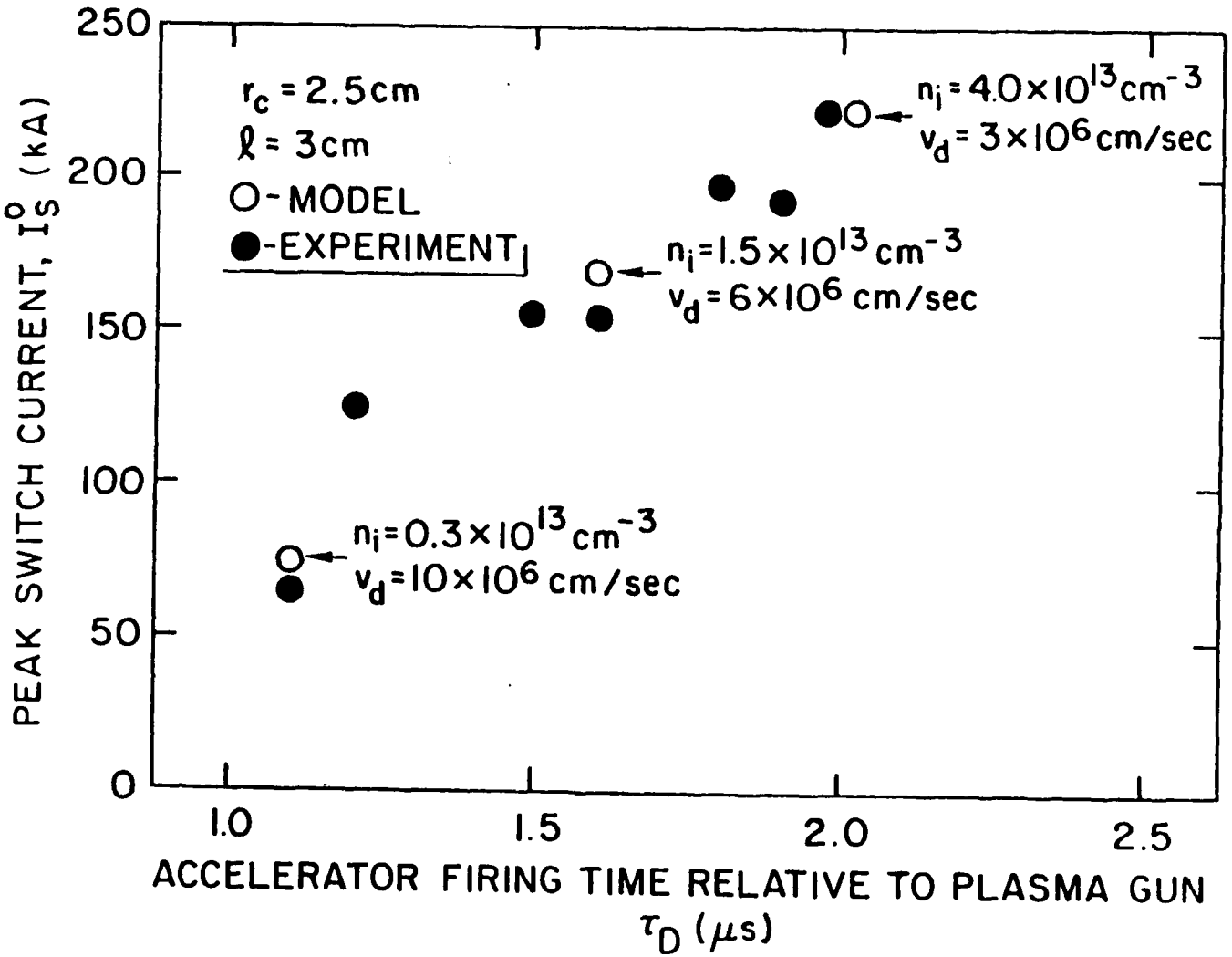

Fig. 9 — Plot of peak switch current, I_S^o ($I_S \equiv I_G - I_L$), as a function of relative delay, τ_D. Also shown are numerical results from the model, using the measured values of n_i and v_d.

$$I_S(t) = (m_i/Zm_e)^{1/2} Zen_e v_d A \qquad (5)$$

where A is the maximum current channel area ($\simeq 2\pi r_c \ell$ for cylindrical geometry) allowed by the switch geometry. At this point the conduction phase ends. A voltage consistent with the Child-Langmuir law, $V_S^{3/2} \propto D_o^2 I_S$, appears across the switch and (depending on L_T and R_L) on the load. For the plasma parameters quoted earlier, $J_i \simeq 30 A/cm^2$. If $A \sim 1000 cm^2$, Eq.(5) predicts a current as high as $I_S \sim$ 3MA may be conducted in this fashion.

Note that in this description of the conduction phase (Fig. 9) there is no $\vec{J}X\vec{B}$ force in the direction of power flow on the load side of the switch plasma until the current channel reaches it. If the opening occurs very rapidly after this instant, the current no longer flows between the electrodes and $\vec{J}X\vec{B} \simeq 0$ in the direction of power flow. Some $\vec{J}X\vec{B}$ related motion on the driver side of the switch plasma will occur as soon as current flows through the switch. This can result in a compression of the plasma and thus an increase in the plasma density, which may affect the switch opening, as discussed next in the section on switch opening. If for this or some other reason the opening occurs very slowly after the current channel broadens to the load side of the switch, the switch plasma will be accelerated in the direction of power flow and a situation similar to that of a plasma accelerator will exist. For this situation, a different regime of physics (which will not be discussed here) is relevant. The switch should be designed so that the fast opening case obtains.

In this picture of conduction, the (small) ion current associated with the injected plasma controls the (large) current the switch will conduct before opening. Thus, for a given A and Z the conduction is essentially controlled by the directed ion flux density to the cathode, $\Gamma_i \equiv n_i v_d$. If

relativistic effects are neglected. Thus, for C^{++}, $I_e/I_i \simeq 100$, and the total current flowing in the switch $I_S = I_e + I_i \simeq I_e$.

The conduction (and opening) phase has been studied in detail by using magnetic probes[32] to obtain spacially and temporally resolved measurements of the magnetic field inside the PEOS in the cylindrical geometry of Fig. (2). These measurements suggest that as the switch current increases, the current channel width at the cathode, ℓ_c in Fig.8, also increases. This increase is predicted by the space charge condition of Eq.(3) with the ion current given by Eq.(2). In cylindrical geometry, we have[33] using Eq.(2) in Eq.(3)

$$\ell_c(t) \simeq \frac{I_S(t)}{(m_i/Zm_e)^{1/2}\, 2\pi r_c J_i} . \tag{4}$$

Because J_i is constant, Eq.(4) predicts that the switch current density ($\simeq I_S/2\pi r_c \ell_c$) will also be constant. This effect is observed.[32] As the switch current increases, the current channel in the plasma is observed to broaden as rapidly as $\ell_c(t)$. The current channel is much larger than the collisionless skin depth, c/ω_{pe}, where c is the speed of light and ω_{pe} is the electron plasma frequency. This implies a resistivity for the plasma during the conduction phase that is much larger than classical and results in a predominantly radial current flow.

The switch will continue to conduct in the manner depicted in Fig. 8 as long as Eq. (4) can be satisfied, i.e., for $\ell_c < \ell$. However, because the generator forces I_S to increase in time while the ion current density is fixed, the switch current eventually reaches a value where the ion current density integrated over the full switch area becomes insufficient to satisfy Eq. (4) i.e., $\ell_c = \ell$. This occurs when

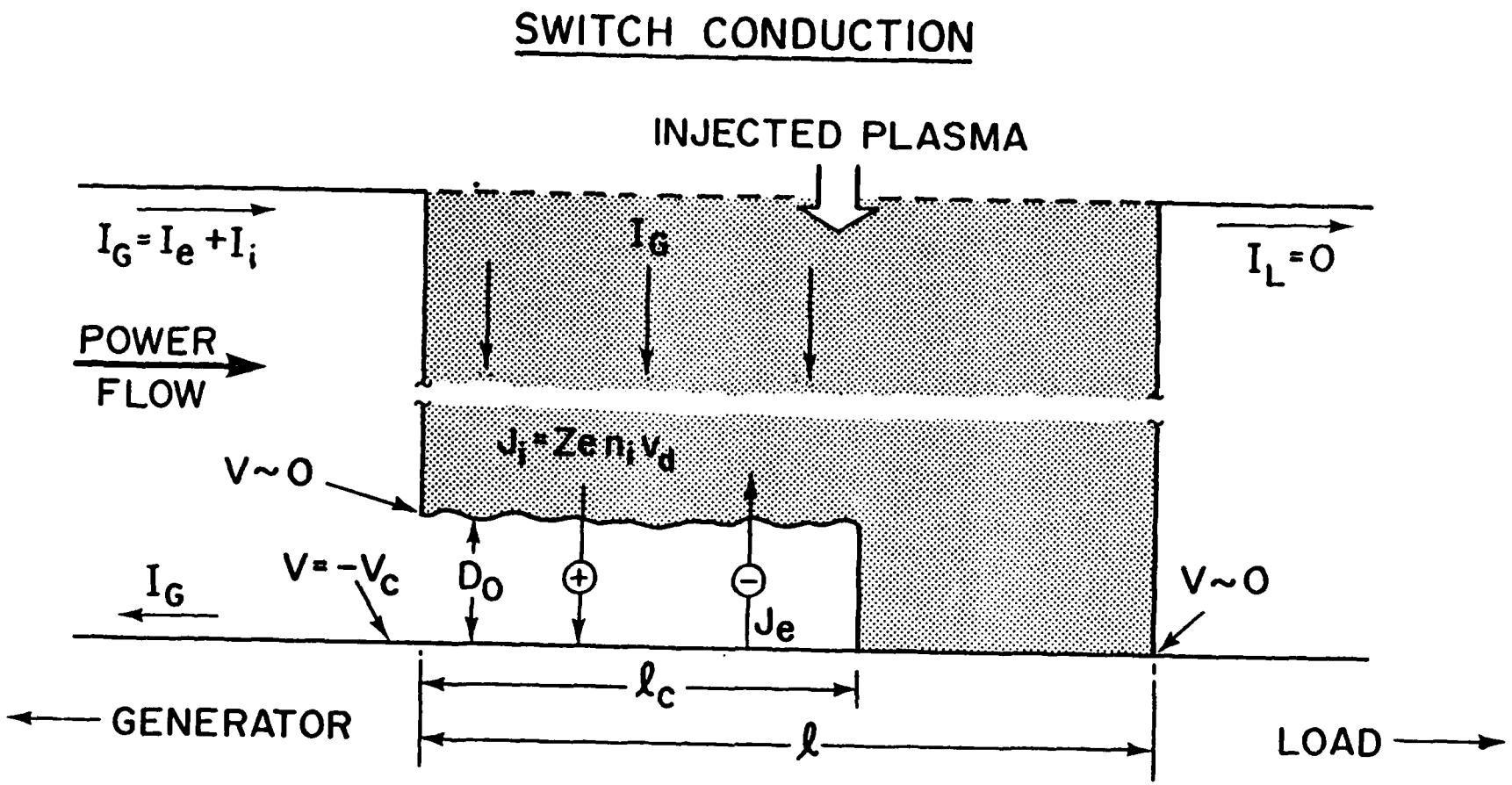

Fig. 8 — Schematic of switch operation during the conduction phase

schematically illustrated in Fig. 8. Initially, the only current flowing through the gap will be ion current associated with the flux of ions from the injected plasma. Very soon, however, the electrostatic field at the cathode becomes large enough[29] that field emission[30] of electrons occurs at the cathode. Electron and ion current are then conducted across the gap in a bipolar space-charge-limited fashion[31]. The ion current density at the plasma-gap boundary is

$$J_i = Zen_i v_d, \tag{1}$$

where n_i is the ion density in the plasma, assumed uniform and constant during conduction and opening, e is the electronic charge, and Z is the ion charge state. The ion drift speed v_d is the average component of ion velocity toward the cathode surface for ions entering the gap. It is usually approximated by the average plasma injection speed. Thus, at any time during conduction the ion current associated with the injected plasma is simply the integral of J_i over the area through which current is flowing. In cylindrical geometry we have

$$I_i \approx 2\pi r_c \ell_c(t) J_i. \tag{2}$$

Note that the switch area is a function of time. For bipolar space-charge-limited flow,[31]

$$\frac{I_i}{I_e} = (Zm_e/m_i)^{1/2}, \tag{3}$$

where I_e is the electron current, $m_e(m_i)$ is the electron (ion) mass, and

value, which depends on only the plasma parameters, the plasma acts as a good conductor [Fig. 1(a)]. The conduction occurs through a non-neutral region, called a sheath or gap, at the cathode in a bipolar space-charge-limited fashion with the electron component emanating from the cathode and the ion component provided by the injected plasma. When the switch current density becomes high enough that the bipolar space-charge condition cannot be satisfied by the ions from the injected plasma, the gap widens, providing more ions. This is called the erosion phase. When the switch current increases to the point where the average electron Larmor radius is comparable with the gap size, the electron lifetime in the gap increases and as a result the space-charge condition is modified in such a way that even more ions are required. This is called the enhanced erosion phase and it is during this phase that the gap widens very quickly. A high voltage is generated across the gap and a substantial fraction of current is diverted to the load. The switch is totally open when the magnetic insulation phase is reached. This occurs at a value of current for which the average Larmor radius is less than the gap size and all the current reaches the load [Fig. 1(c)]. A more detailed explanation now follows.

A. Switch Physics

1. Switch Conduction

As described in the previous section, a plasma is injected into the switch region and after a time τ_D the generator is fired applying a high voltage to the cathode, $-V_C$. This voltage causes a non-neutral region or gap of dimension D_o (typically, D_o >> Debye length) to be formed at the cathode surface. The situation at one instant during the switch conduction is

will appear mostly across a sheath or gap between the plasma and the cathode. The actual flow of current through the plasma is associated with drift motion. One may define an effective "switch resistance" as the ratio of the voltage across the switch to the current flowing through it. However, this quantity will not necessarily be related to the resistivity of the plasma, which determines the fraction of the total energy dissipated by the switch in heating of the switch plasma. Most of the kinetic energy acquired by electrons that traverse the cathode sheath is lost to the anode when those electrons leave the system. The electrical equivalent of the switch behavior will be primarily determined by the cathode sheath physics.

A description of the PEOS operation was introduced, although in a non-switching context, by Miller et al.,[27] honed by Mendel et al.,[18] significantly modified by Meger, et al.[10] and later described more fully and compared closely to experiment by Ottinger, et al.[28] This description is a blend of theoretical ideas and experimental observations. It describes the observed quantitative behavior of the PEOS[30] and has been successfully used to make qualitative predictions. The PEOS physics is briefly summarized in the next paragraph. A more detailed explanation and justifications for assumptions made, along with a discussion of physics constraints on system design, follow in parts A and B respectively.

The operation is most easily described as a sequence of four phases: conduction, erosion, enhanced erosion, and magnetic insulation. The last three phases constitute the switch opening. Effects related to $\vec{J}\times\vec{B}$ body forces and high density plasma associated with plasma-wall interaction or field emission are neglected here but will be discussed in what follows. The plasma is injected into the switch region and voltage applied to the cathode. As long as the switch current density remains below a predictable

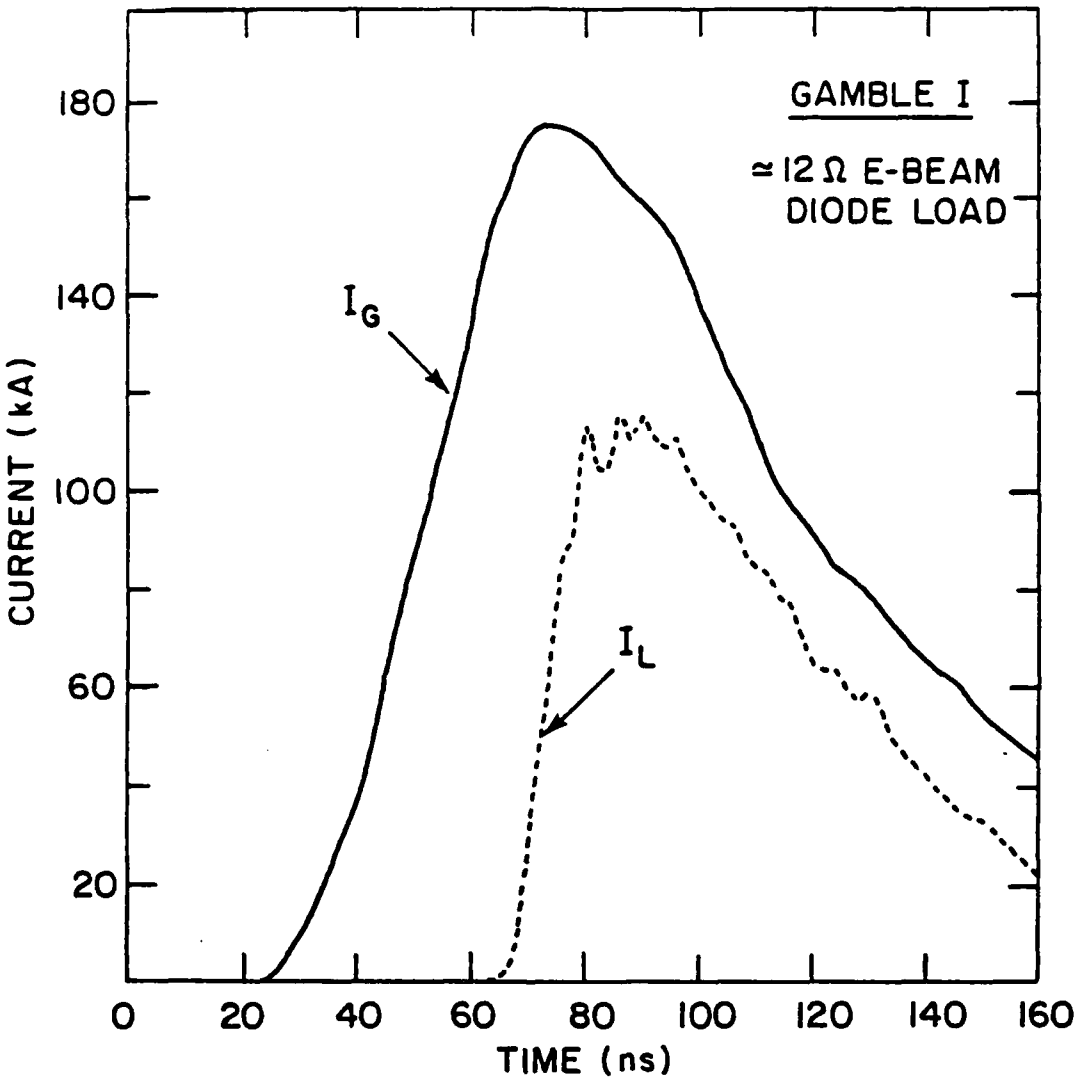

Fig. 7 — Measured currents flowing through the generator (I_G) and load (I_L) for Gamble I with an e-beam diode load

require a finite R_L. Some of these applications utilize an e-beam diode for the load. Data[10] from Gamble I using a nominal 12-Ω e-beam diode load are shown in Fig. 7. The geometry is identical to Fig. 2(a). The load current rises in $\lesssim$ 10ns. However, for this example the peak load current only reaches about 65% of the peak generator current and I_L never reaches I_G, both in contrast to the short circuit case of Fig. 3. This current loss results in a reduction of the maximum power that can be delivered to the load. The cause of the current loss is rooted in the physics of the switch system.[26] As with most opening switches, the PEOS and the system strongly interact in such a way as to adversely affect the switch performance. By understanding the nature of the interaction, however, the losses illustrated in Fig. 7 can be minimized[26] (see Sec. III-B).

III. Principles of Operation

The operation of any opening switch can be conveniently divided into two parts: conduction, [Fig. 1(a)], and opening [Figs. 1(b) and (c)]. During conduction the switch isolates the load from the rest of the system. In inductive-store applications the switch typically conducts for the time it takes to energize an inductor. When the switch opens, the current is rapidly diverted to the load. Any description of the PEOS operation must explain these switch properties as well as the rest of the phenomenology described in the previous section.

It is important to recognize at the outset that the PEOS conducts a large current ($\sim$ MA) across a strong magnetic field ($\gtrsim$ 10kG) and diverts this current to a finite resistance load using a plasma for which the classical electron-ion momentum transfer time is much longer than either the electron cyclotron period or (in most cases) the time scale of switch operation ($\sim$ 100 ns) . Also, because of Debye shielding, the voltage across the plasma

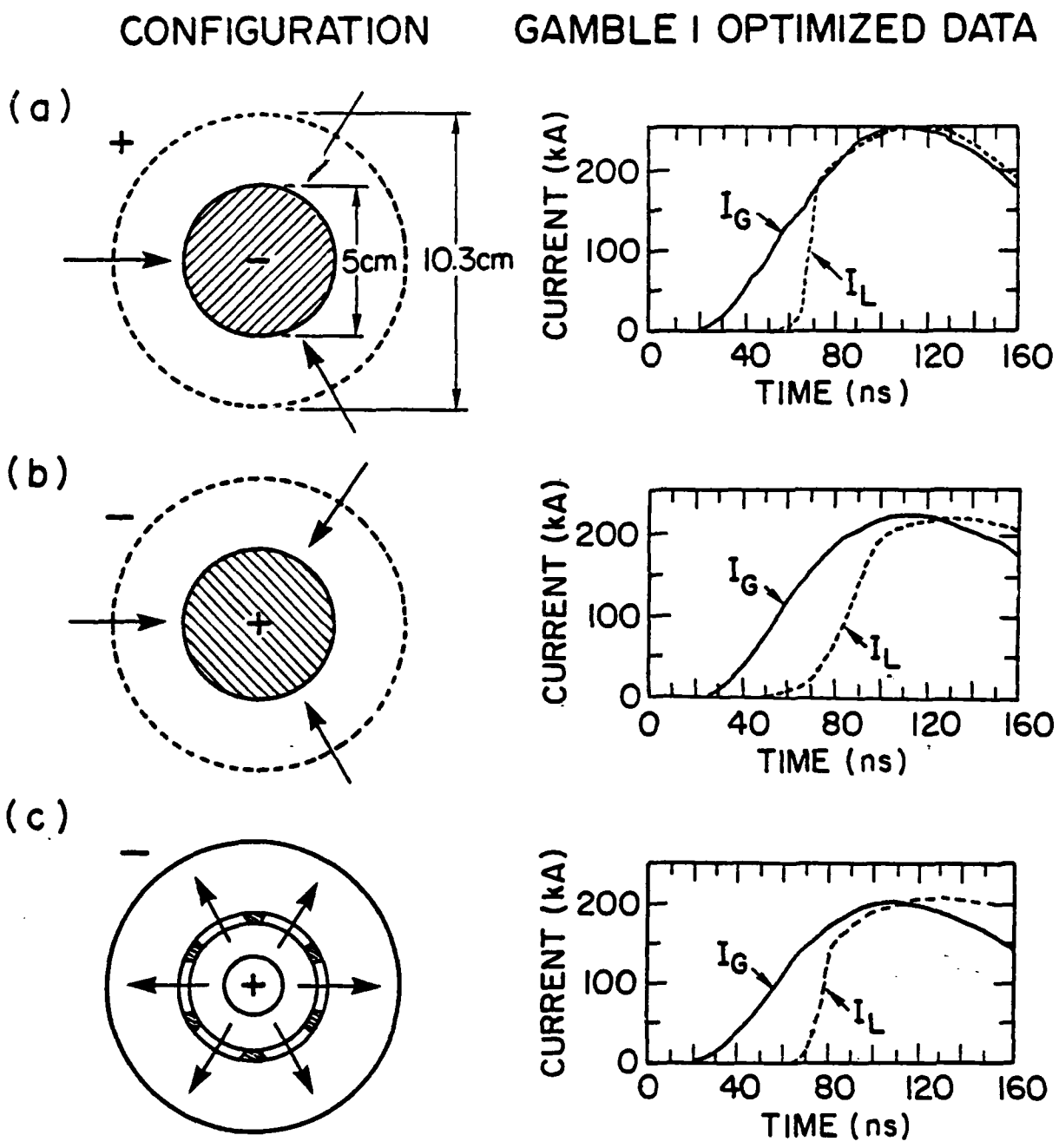

Fig. 6 — Illustration of Gamble I system geometry and data for various plasma injection/electrode polarity configurations: (a) inward injection toward cathode, (b) inward injection toward anode and (c) outward injection toward cathode.

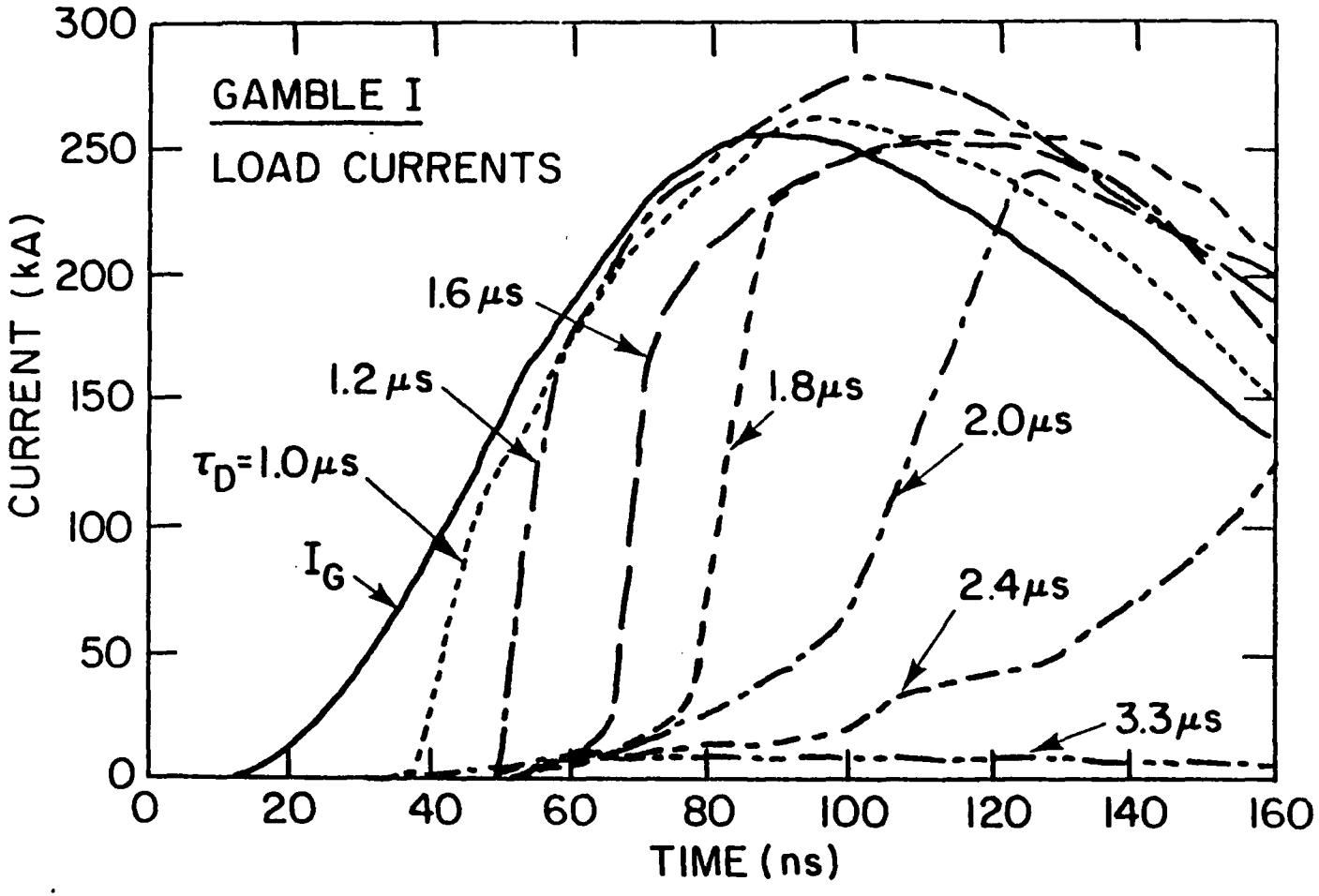

Fig. 5 — Plots of load currents, I_L, as a function of time for various time intervals between the plasma gun and generator firing, τ_D. Also shown is a typical generator current, I_G. Data are from Gamble I with a short circuit load.

increased and the required ion current is greatly enhanced[36] over that given in Eq. (3). The new condition is[36]

$$\frac{I_i}{I_e} \approx \left[2m_e Z(\gamma + 1)/m_i\right]^{1/2} \frac{\ell}{D} \tag{8}$$

and the gap must open faster to provide the additional required ion current. This is called the enhanced erosion phase [Fig. 10(b)] and is responsible for the observed rapid switch opening. Equation (8) now determines I_i in Eq. (6) and erosion rates of $dD/dt \sim 10^8$ cm/s can be obtained. For $\gamma^2 >> 1$, Eq. (7) gives $V_S \propto I_S D$. Thus, as I_S and D increase, V_S also increases, forcing more current through the load.

Depending on the geometry, the magnetic field may vary along the switch length. Thus, electrons flowing across one part of the switch gap may experience a smaller magnetic field than those flowing across another part of the gap. When the load current becomes large enough that the magnetic field prevents electrons from traversing the gap anywhere, the switch is said to be magnetically insulated. This is the last phase of the switch opening and is depicted in Fig. 10(c). When $I_L \gtrsim I_C$, the electrons are completely insulated so that $I_e = 0$, $I_S = I_i << I_C$, and the switch is open. The ion current is no longer enhanced because the magnetic field now holds the electron trajectories close to the cathode surface and I_i is simply the one species space-charge-limited current for ions.

To summarize the PEOS model, the PEOS remains closed during the conduction phase with the switch area and ion flux density from the injected plasma determining the peak switch current. The switch opening commences with the erosion phase, accelerates during the enhanced erosion phase and ends with the magnetic insulation phase. The transition of I_i from bipolar flow [Eq.

(3)] to enhanced flow [Eq. (8)] back to single species flow can be modeled in a continuous way.[37] A comparison of the measured time histories of I_G and I_L for Gamble I (nominal 10-Ω e-beam diode load) with those computed using this model is shown in Fig. 11. The model correctly predicts the observed conduction and opening characteristics.

Throughout this discussion $\vec{J}X\vec{B}$ forces have been assumed to be negligible in opening the gap. In the coaxial geometry of Fig. (2), magnetic field measurements[32] reveal that the current predominantly flows in the radial direction, suggesting small radial $\vec{J}X\vec{B}$ forces. Moreover, calculations for coaxial geometry that assume the current flows in a thin channel parallel to the axis before going radially to the cathode result in a time history and density scaling for opening that is not supported by experiment. The description of the conduction phase presented earlier asserts that $\vec{J}X\vec{B}$ forces perpendicular to the current flow will have negligible effect on the switch behavior as long as the current channel length increases more rapidly and the switch opens faster than the time for these forces to significantly accelerate the plasma. The magnetic field measurements on Gamble I indicate that axial $\vec{J}X\vec{B}$ forces are not significant[32], in accordance with this assertion. However, experiments are needed to more fully explore the long conduction time (> 100 ns), high current ($\gtrsim$ MA) regime.

As discussed earlier in this section, for a given A and Z the directed ion flux density to the cathode, $\Gamma_i = n_i v_d$, controls how much current the switch will conduct before the erosion phase begins. How well the switch opens, on the other hand, will be determined by the gap size relative to the characteristic electron Larmor radius. Assuming $v_d \ll dD/dt$, Eq. (6) gives

$$\frac{dD}{dt} \simeq \frac{I_i}{Zen_iA} \cdot \tag{9}$$

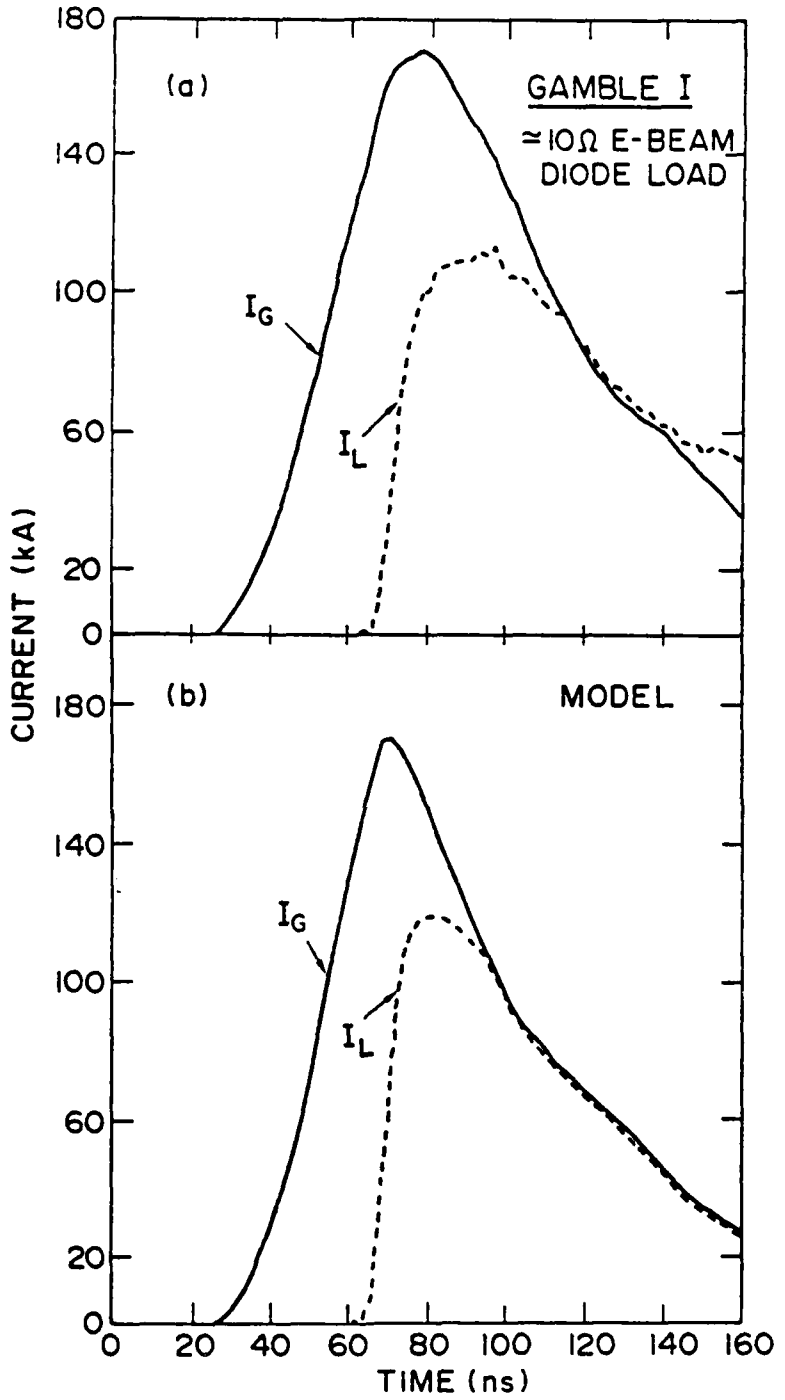

Fig. 11 — Comparison of measured and calculated time histories for generator (I_G) and load (I_L) currents

Thus, for a given value of I_i, A, and Z, the rate at which the gap opens $\propto n_i^{-1}$. In order to achieve a high conduction current $\Gamma_i A$ must be large [Eq. (5)] - but to achieve rapid opening and large final gap size n_i must be small [Eq. (9)]. This implies v_d must be large to have both high conduction current and these good opening characteristics. Present plasma sources[19,20] have $Ze\Gamma_i \approx 30 A/cm^2$ with $n_i \approx 10^{13} cm^{-3}$ and $v_d \approx 10^7 cm/s$. An important area of research is the development of plasma sources with similar or greater Γ_i but with lower n_i. For a given switch configuration, the optimum lower bound on n_i is determined from $\vec{J}x\vec{B}$ force considerations. The effect of varying n_i and v_d while keeping Γ_i fixed is illustrated in Fig. 12, which is a result of a computation for Gamble I parameters using the model just described.[28,38] Although the current at which the switch begins to open remains the same, the best switch performance is obtained with the highest v_d and lowest n_i [Fig. 12(a)]. This behavior has been confirmed in the laboratory. The plasma injection geometry will also affect the value of Γ_i, which explains the data in Fig. 6. For example, in Fig. 6(b), the flow velocity is toward the anode resulting in v_d and n_i at the cathode that are different from the cases illustrated in Figs. 6(a) and (b). Control of the PEOS behavior is strongly dependent on the "quality" of the directed flux to the cathode - a "high quality flux" having, for a given $\Gamma_i A$, a low n_i and high v_d.

B. System Considerations

In order for the switch to operate in the most efficient way; i.e., for

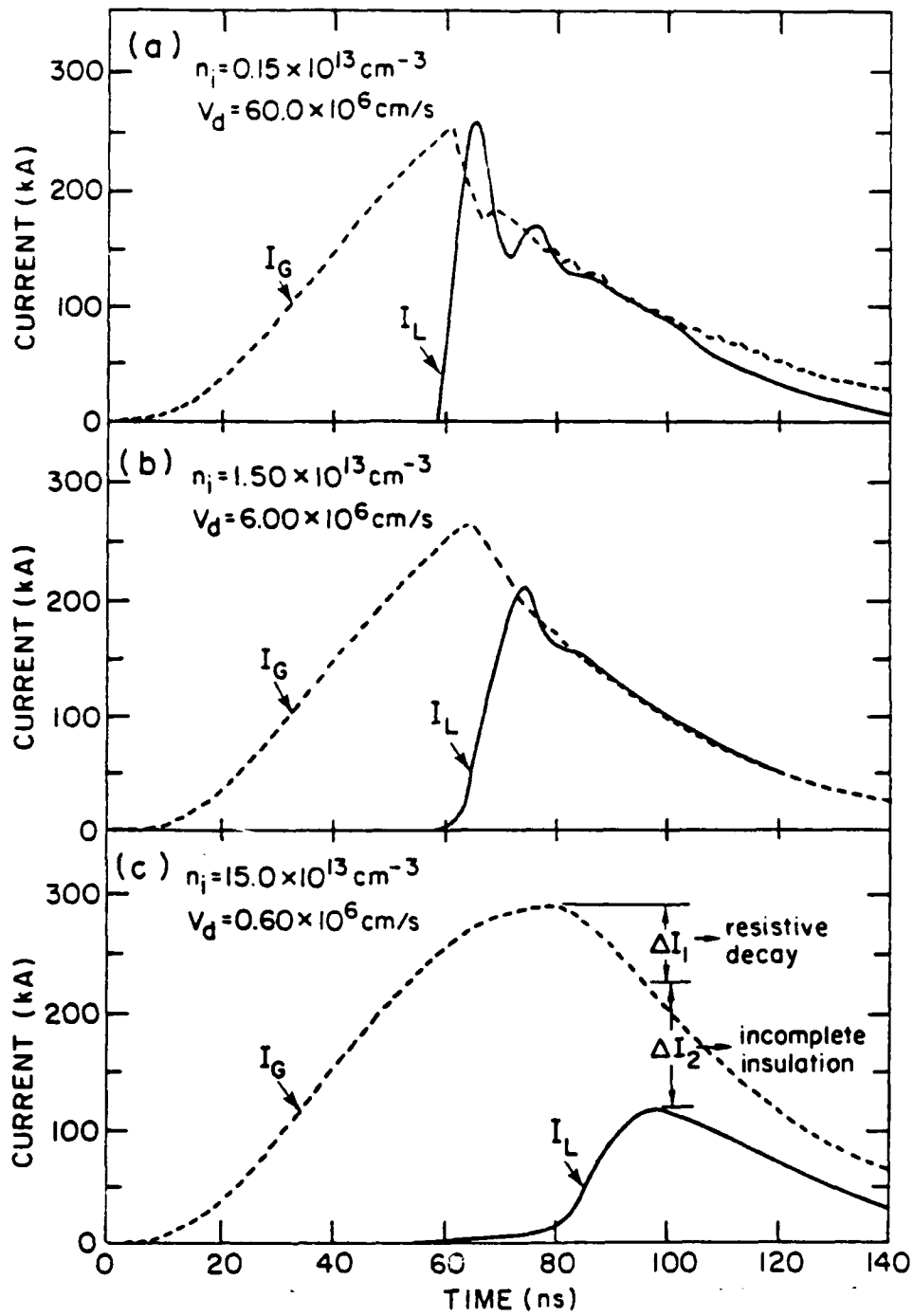

Fig. 12 — Results of numerical computations based on the PEOS model showing the effects of varying the values of n_i and v_d while keeping the product fixed. The load is a fixed 6Ω resistor.

as much of the stored inductor current to reach the load as is permitted by magnetic flux conservation, two conditions must be met. First, the switch must open in a time that is fast compared with the characteristic resistive decay time of the current during opening. This is equivalent to saying that magnetic flux be very nearly conserved during the opening. Second, the electrons in the gap must be totally insulated. The final switch gap must be large compared with the characteristic electron Larmor radius in the gap or, equivalently, $I_L \gtrsim I_c$. If these two conditions are not met, then the situation depicted in Fig. 12(c) may arise. There, the generator current at the time of peak load current is much less than the peak generator current [(ΔI_1 of Fig. 12(c)] because the opening is slow compared with the current decay time during opening. A reduction in current of only 5% would be expected from magnetic flux conservation. There is also a loss of current to the load as evidenced by the finite difference between generator and load current after opening [ΔI_2 of Fig. 12(c)], resulting from incomplete insulation. This loss is also evident in Fig. 7, where $I_G > I_L$ after opening, indicating current is still flowing through the switch.

These two conditions can be combined to define an operational window for PEOS systems. An example of a result of this analysis[39] for the Gamble I generator is shown in Fig. 13. Here the accessible load voltages, V_L, are plotted as a function of the load resistance R_L, for an assumed switching time, $\tau_S \sim I_L(dI_L/dt)^{-1}$, storage inductance, L_o, and ratio of cathode radius to final gap size, r_c/D. The dotted line in Fig. 13 represents the maximum voltage that can be generated at the load, $V_L = R_L I_L$, consistent with resistive decay of the current during opening. The characteristic resistive decay time for the current is $\sim L_o/R$, where R is some effective system resistance during opening. V_L can not be higher than this dotted line for a

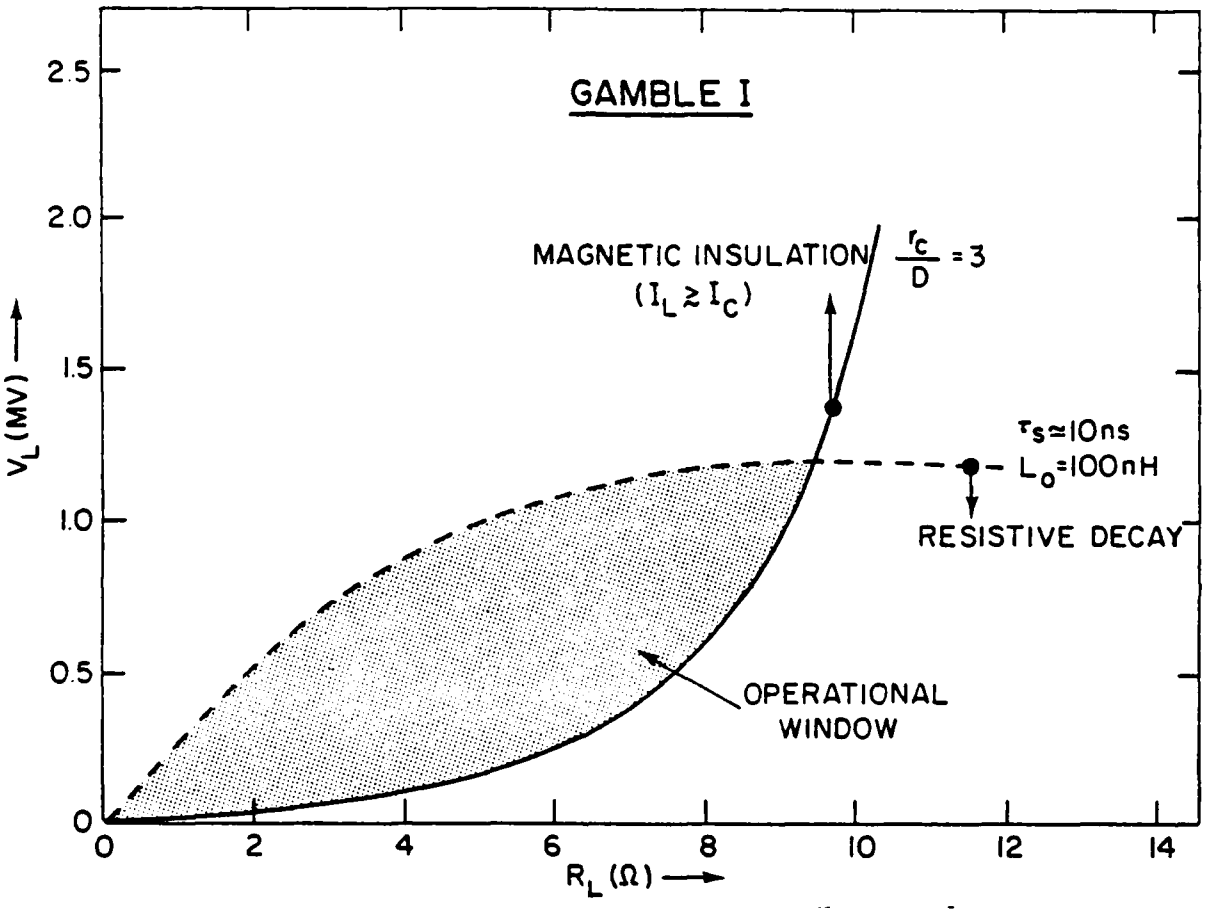

Fig. 13 — Operational window for a PEOS system on the Gamble I device for L_o = 100 nH, r_c/D = 3, and τ_S = 10 ns. Regime of efficient operation (minimum current loss) is area between dotted and solid line.

given R_L. Here, how efficiently the generator energizes the storage inductance has also been included. This efficiency can be as high as 80%, depending on the value of L_o. The solid line is obtained by requiring magnetic insulation, i.e., $I_L (= V_L/R_L) = I_c$. To minimize current loss, the switch electrons must be insulated in the gap. For a given R_L, I_L must be large enough that V_L lie at or above the solid line. Thus for a given τ_s, L_o, and r_c/D the region between the dotted and solid lines (shaded portion of Fig. 13) represents an operational window for efficient system operation.

If D is increased (for a given r_c), it takes less current to insulate the electrons and therefore V_L will be smaller for a given R_L. This shifts the solid line in Fig. 13 to the right and down from the one shown. If τ_s is decreased (for a given L_o) the maximum current available to the load for a given R_L increases because the switching time becomes small compared with L_o/R. This increases the maximum accessible V_L for a given R_L, resulting in the dashed line in Fig. (13) shifting up from the one shown. Thus the system is optimized by making D as large and τ_s as small as possible. In practice, D and τ_s are themselves optimized through proper choice of plasma parameters (small n_i, large v_d) as discussed in Sec. III-A [Eq.(9)].

This analysis illustrates the complex interactive nature of this switch system. In general, the strong interaction between the pulsed power system and opening switch is a characteristic of most inductive store systems, regardless of the particular opening switch employed. By properly designing the system and choosing the switch plasma parameters, current loss for a given application can be eliminated or at least minimized. Other loss mechanisms not addressed in the foregoing analysis are possible. For example, current loss can occur in the transition region between the switch and load. This effect will not be discussed here except to say that it has been shown

experimentally that this loss can also be minimized.[26]

IV. Applications

The PEOS has a wide variety of applications in fields of research and development that require power conditioning at high power levels ($\gtrsim$ 1 TW). Three applications of current interest will be briefly reviewed here.

One of the most exciting applications involves the adaptation of a PEOS inductive-store/pulse-compression system to state-of-the-art generators to produce a higher power, higher voltage, shorter risetime pulse than can otherwise be obtained from the generator. This application is loosely termed power and voltage multiplication and has particular relevance in Light Ion Beam Inertial Confinement Fusion (LIBICF) research.[5,6-9] Fast risetime and high voltage are particularly attractive for LIBICF because of the required short pulses (10-20 ns) and ion energies as high as ≈ 30 MeV (for lithium ions).

The potential for significant power and voltage multiplication was first demonstrated by Meger et al.[10] The data in Fig. 14 serve to illustrate the salient features of this application, albeit under non-optimized conditions. The data shown are the power to the load, P_L, the load voltage, V_L, and the energy delivered to the load, E_L, as functions of time for three cases: (1) Gamble I configured with the PEOS inductive-store/pulse-compression system shown in Fig. 2(a) and an e-beam diode load of nominally Ω ; (2) Gamble I configured with a matched, 2-Ω constant resistance load (as a practical matter, a minimum of ≈ 30 nH separates the generator from the load in this configuration); and (3) Gamble I configured with a 6-Ω constant resistance overmatched load (again with ≈ 30 nH of inductance between the generator and load). The data for the first case was obtained from a Gamble I shot. The

measured generator voltage waveform for that particular shot was used to calculate the parameters for the other two cases. The risetimes of both P_L and V_L with the PEOS system are ≈ 10 ns, compared with ≈ 50 ns for the conventionally configured systems. V_L is a factor ~ 2 higher with the PEOS system compared with the matched load and slightly higher than the overmatched case; however, P_L is twice as high with the PEOS system compared with the overmatched case. For case 1, a current loss (discussed earlier) of ≈ 23% was observed, which accounts for the peak P_L with the PEOS being comparable with the matched load case. Power multiplication over the peak matched load power of ~ 1.5 could have been obtained at ~ 1.4 times the overmatched load voltage if all the current went to the load.

The cost associated with achieving power and voltage multiplication is illustrated in the bottom graph of Fig. 14. For the (non-optimized) shot illustrated, the PEOS system delivers ≈ 66% of the energy that could be delivered to a matched load. Note, however, that in the first 20 ns of the pulse, the PEOS system delivers twice as much energy to the load as the matched load case during the same time interval. There is presently a research effort at NRL directed toward improving the current transfer so that significant power and voltage multiplication can be obtained with a minimum cost in energy. This effort focuses on: (1) the development of new plasma sources which can provide a higher quality flux than is presently available from the sources now used and (2) making best use of the present sources through optimization of the system geometry. Recent calculations suggest that the PEOS system could give a factor ~ 2 power multiplication and ~ 4 voltage multiplication over matched-load values with the present sources for Gamble I parameters if the proper system geometry could be used.

With the hope of attaining some degree of power multiplication, initial

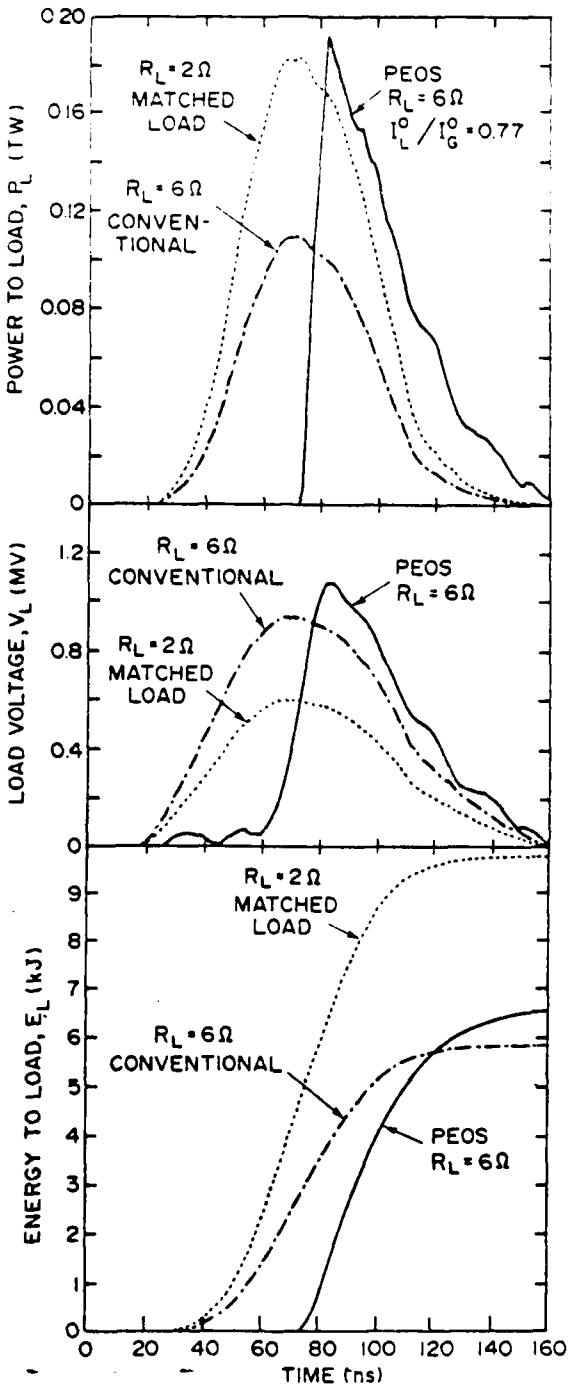

Fig. 14 — Sample data from Gamble I illustrating some advantages that a generator configured with a PEOS inductive store/pulse compression system has over a conventionally configured generator with both a matched load (2Ω) and an overmatched load (6Ω)

PEOS experiments on the Particle Beam Fusion Accelerator I (PBFA I) at Sandia National Laboratories were performed.[5,6,9]. In these experiments the PEOS was additionally used to minimize the effects of intermodule jitter, symmetrize power flow, and narrow the pulse width. The experiments were successful in the latter three areas. Current loss in the switch and between the switch and load prevented increased power to the load.[5,6] PBFA II,[6,9] which is presently under construction, is being designed from the start to take advantage of inductive-store/pulse-compression techniques. For PBFA II, the PEOS must transfer≈ 6 MA in ≈ 10 ns generating ≈ 30 MV in a 5-Ω load. Calculations indicate that with proper system design and a small extension of present plasma source technology these requirements can be met.

Another application involves adapting the PEOS to a conventional generator, primarily to reduce prepulse, provide a shorter rise-time pulse, and improve the symmetry of the power flow. Here, a large vacuum inductive store region is not necessary. In addition to the impact on ICF discussed in the previous paragraph, this application has particular relevance to ion diode physics[13,15,16] and the generation of imploding z-pinch plasmas.[12,14,17] Experiments at Physics International Corporation[14,17] using imploding wire arrays and at NRL[12] using annular gas puffs indicate an improvement in the quality of the implosions (better axial uniformity, smaller pinch radius, etc.) when the PEOS is used. The NRL group also reports that K-line radiation from neon pinches can be up to 2.5 times higher with the PEOS than without the PEOS at the same current level.[12] Although a detailed understanding of these phenomena is still forthcoming, the preliminary experimental results are encouraging.

The final application considered here, and potentially the one with the most impact on the development of pulsed power, focuses on the eventual elimination of conventional generators from the pulsed-power system

altogether. Such generators usually employ a Marx type configuration of capacitors as a prime energy store in conjunction with a water (or oil) dielectric pulse-forming line. They require large quantities of oil and high-purity water for high voltage insulation and they employ a high voltage (> 1 MV) vacuum interface. These generators tend to be very large and do not scale economically to high energy($\gtrsim$ 20 MJ) systems. One alternative system utilizes either a low voltage($\sim$ 50 kV), compact, high energy density capacitor bank[4,40,41] or a homopolar generator[2] to slowly ($10\text{-}10^3$ μs) energize a vacuum inductor, after which a series of opening switches successively increases the voltage and decreases the pulse risetime. A critical element in this program is the development of the required opening switch technology. The PEOS is a prime candidate for the final opening switch in such a system. This work is just coming out of its infancy and should provide interesting results in the near future.

The authors would like to thank F.C. Young, I.M. Vitkovitsky, J.D. Sethian and R.F. Fernsler for their helpful comments. This work was supported by Sandia National Laboratories, the Department of Energy, the Defense Nuclear Agency and the Office of Naval Research.

References

1. S. A. Nasar and H. H. Woodson, Proceedings of the Sixth Symposium on Engineering Problems of Fusion Research, San Diego, CA, IEEE Pub. No. 75CH1097-5-NPS, 316 (1975).

2. R. D. Ford, D. Jenkins, W. H. Lupton and I. M. Vitkovitsky, Rev. Sci. Instrum. 52, 694 (1981).

3. K. D. Bergeron and J. Pace VanDevender, 1978 IEEE International Conference on Plasma Science, Monterey, CA, (1978), IEEE Cat. No. 78CH1357-3NPS,p. 261.

4. P. F. Ottinger, R. J. Commisso, W. H. Lupton and J. D. Shipman, Jr., Fifth IEEE Pulsed Power Conference, Washington, DC (1985), to be published.

5. R. W. Stinnett, W. B. Moore, R. A. Meger, J. M. Neri and P. F. Ottinger, Bull. Am. Phys. Soc. 29, 1207 (1984).

6. J. P. VanDevender, et al., Tenth International Conference on Plasma Physics and Controlled Nuclear Fusion Research, London, U.K. (1984).

7. K. Imasaki, et al., Tenth International Conference on Plasma Physics and Controlled Nuclear Fusion Research, London, U. K. (1984).

8. R. A. Meger, J. R. Boller, R. J. Commisso, G. Cooperstein, S. A. Goldstein, R. Kulsrud, J. M. Neri, W. F. Oliphant, P. F. Ottinger, T. J. Renk, J. D. Shipman, Jr., S. J. Stephanakis, B. V. Weber and F. C. Young, Fifth International Conference on High-Power Particle Beams, San Francisco, CA (1983), p.330.

9. J. Pace VanDevender, Fifth International Conference on High Power Particle Beams, San Francisco, CA (1983), proceedings, p. 17.

10. R. A. Meger, R. J. Commisso, G. Cooperstein and Shyke A. Goldstein, Appl. Phys. Lett. 42, 943 (1983).

11. R. A. Meger, J. R. Boller, D. Colombant, R. J. Commisso, G. Cooperstein, S. A. Goldstein, R. Kulsrud, J. M. Neri, W. F. Oliphant, P. F. Ottinger, T. J. Renk, J. D. Shipman, Jr., S. J. Stephanakis, F. C. Young and B. V. Weber, Fourth IEEE Pulsed Power Conference, Albuquerque, NM, (1983), Digest of technical papers, (IEEE Cat. No. 83CH1908-3), p. 335.

12. S. J. Stephanakis, S. W. McDonald, R. A. Meger, P. F. Ottinger, F. C. Young, C. G. Mehlman, J. P. Apruzese and R. E. Terry, Bull. Am. Phys. Soc. 29, 1232 (1984).

13. S. J. Stephanakis, T. J. Renk, G. Cooperstein, Shyke A. Goldstein, R. A. Meger, J. M. Neri, P. F. Ottinger and F. C. Young, Bull. Am. Phys. Soc. 28, 1055 (1983).

14. R. Stringfield, P. Sincerny, S.-L. Wong, G. James, T. Peters and C. Gilman, IEEE Trans. Plasma Sci. PS-11, 200 (1983).

15. R. A. Meger and F. C. Young, J. Appl. Phys. 53, 8543 (1982).

16. W. F. Oliphant, S. J. Stephanakis, G. Cooperstein, Shyke A. Goldstein, R. A. Meger, D. D. Hinshelwood and H. U. Karow, 1981 IEEE International Conference on Plasma Science, Santa Fe, NM, (1981), IEEE Cat. No. 81CH1640-2NPS, p. 81

17. R. Stringfield, R. Schneider, R. D. Genuario, I. Roth, K. Childers, C. Stallings and D. Dakin, J. Appl. Phys. 52, 1278 (1981).

18. C. W. Mendel, Jr. and S. A. Goldstein, J. Appl. Phys. 48, 1004 (1977).

19. T. J. Renk, S. J. Stephanakis, R. A. Meger and J. R. Boller, Bull. Am. Phys. Soc. 28, 1055 (1983).

20. C. W. Mendel, Jr., D. M. Zagar, G. S. Mills, S. Humphries, Jr. and S. A. Goldstein, Rev. Sci. Instrum. 51, 1641 (1980).

21. G. Cooperstein, J. J. Condon and J. R. Boller, J. Vac. Sci. Tech. 10, 961 (1973).

22. R. J. Commisso, Shyke A. Goldstein, R. A. Meger, J. M. Neri, W. F. Oliphant, P. F. Ottinger, F. C. Young and B. V. Weber, Bull. Am. Phys. Soc. 28, 1147 (1983).

23. B. V. Weber, R. J. Commisso, W. F. Oliphant and P. F. Ottinger, 1984 IEEE Conference on Plasma Science, St. Louis, MO (1984), IEEE Cat. No. 84CH1958-8, p.8.

24. J. M. Neri, R. J. Commisso, Shyke A. Goldstein, P. F. Ottinger, B. V. Weber and F. C. Young, 1983 IEEE Conference on Plasma Science, San Diego, CA (1983), Conference record - Abstracts (IEEE Cat. No. 83CH1947-3), p. 124.

25. J. M. Neri, R. J. Commisso and R. A. Meger, Bull. Am. Phys. Soc. 27, 1054 (1982).

26. R. J. Commisso, D. D. Hinshelwood, J. M. Neri, F. W. Oliphant, T. J. Renk and B. V. Weber, Bull. Am. Phys. Soc. 29, 1206 (1984).

27. P. A. Miller, I. W. Poukey and T. P. Wright, Phys. Rev. Lett. 35, 940 (1976).

28. P. F. Ottinger, S. A. Goldstein and R. A. Meger, J. Appl. Physics 56, 774 (1984).

29. D. D. Hinshelwood, private communication.

30. D. D. Hinshelwood, NRL Memorandum Report No. 5492 (1985); R. K. Parker, R. E. Anderson and C. V. Duncan, J. Appl. Physics 45, 2463 (1974).

31. I. Langmuir and K. B. Blodgett, Phys. Rev. (Ser. 2) 22, 347 (1923); I. Langmuir, Phys. Rev. (Ser. 2) 2, 450 (1913).

32. B. V. Weber, R. J. Commisso, R. A. Meger, J. M. Neri, W. F. Oliphant and P. F. Ottinger, Appl. Phys. Lett. 45, 1043, (1984).

33. B. G. Mendelov, J. Tech. Phys. USSR 21, 710 (1951).

34. W. Koch, Z. Tecn. Phys. 17, 446 (1936).

35. R. J. Barker and Snyke A. Goldstein, Bull. Am. Phys. Soc. 26, 921 (1981).

36. Shyke A. Goldstein and R. Lee, Phys. Rev. Lett. 35, 1079 (1975).

37. K. D. Bergeron, Appl. Phys. Lett. 28, 306 (1976).

38. P. F. Ottinger, J. Grossmann, J. Neri, R. Kulsrud, D. Bacon and A. T. Drobot, Bull. Am. Phys. Soc. 29, 1342 (1984).

39. P. F. Ottinger, R. A. Meger and J. Neri, 1984 IEEE International Conference on Plasma Science, St. Louis, MO (1984), IEEE Cat. No. 84CH1958-8, p. 8.

40. R. D. Ford J. K. Burton, R. J. Commisso, G. Cooperstein, J. M. Grossmann, D. J. Jenkins, W. H. Lupton, J. M. Neri, P. F. Ottinger and J. D. Shipman, Jr., Fifth IEEE Pulsed Power Conference, Washington, DC (1985), to be published.

41. D. K. Haskell and J. A. Sevigny, Fifth IEEE Pulsed Power Conference, Washington, DC (1985), to be published; J. Shannon, M. Wilkerson. R. Miller and O. Cole, ibid.

DISTRIBUTION LIST

Director
Defense Nuclear Agency
Washington, DC 20305
Attn: TISI Archieves — 1 copy
TITL Tech. Library — 3 copies
J. Z. Farber (RAEV) — 1 copy
C. Shubert (RAEV) — 1 copy
J. Benson (RAEV) — 1 copy

U.S. Department of Energy
Division of Inertial Fusion
Washington, DC 20545
Attn: L. E. Killion — 1 copy
M. Sluyter — 1 copy
R.L. Schriever — 1 copy

U.S. Department of Energy
Office of Classification
Washington, DC 20545
Attn: Robert T. Duff — 1 copy

U.S. Department of Energy
Nevada Operations Office
Post Office Box 14100
Las Vegas, NV 89114
Attn: Rex Purcell — 2 copies

U.S. Department of Energy
P.O. Box 62
Oak Ridge, TN 37830 — 2 copy

Air Force Office of Scientific Research
Physics Directorate
Bolling AFB, DC 20332
Attn: H. Pugh — 1 copy
R. J. Barker — 1 copy

Air Force Weapons Laboratory, AFSC
Kirtland AFB, NM 87117
Attn: NTYP (W. L. Baker) — 1 copy

Atomic Weapons Research Establishment
Building H36
Aldermaston, Reading RG 7 4PR
United Kingdom
Attn: J.C. Martin — 1 copy

Boeing Company, The
P.O. Box 3707
Seattle, WA 98124
Attn: Aerospace Library — 1 copy

Brookhaven National Laboratory
Upton, NY 11973
Attn: A.F. Maschke — 1 copy

BMO/EN
Norton AFB, CA
Attn: ENSN — 1 copy

Commander
Harry Diamond Laboratory
2800 Powder Mill Rd.
Adelphi, MD 20783
(CNWDI-INNER ENVELOPE: ATTN: DELHD-RBH)
Attn: DELHD-NP — 1 copy
DELHD-RCC -J.A. Rosando — 1 copy
DRXDO-RBH -J. Agee — 1 copy
DRXDO-TI - Tech Lib. — 1 copy

Cornell University
Ithaca, NY 14850
Attn: D.A. Hammer — 1 copy
R.N. Sudan — 1 copy

Defense Advanced Research Project Agency
1400 Wilson Blvd.
Arlington, VA 22209
Attn: R. L. Gullickson — 1 copy

Defense Technical Information Center
Cameron Station
5010 Duke Street
Alexandria, VA 22314
Attn: T.C. — 2 copies

JAYCOR, Inc.
205 S. Whiting Street
Alexandria, VA 22304
Attn: D. D. Hinshelwood — 1 copy
P. F. Ottinger — 1 copy
B. V. Weber — 1 copy
J. M. Grossmann — 1 copy

Kaman Tempo
816 State Street (P.O. Drawer QQ)
Santa Barbara, CA 93102
Attn: DASIAC 1 copy

KMS Fusion, Inc.
3941 Research Park Drive
P.O. Box 1567
Ann Arbor, MI 48106
Attn: Alexander A. Glass 1 copy

Lawrence Berkeley Laboratory
Berkeley, CA 94720
Attn: D. Keefe 1 copy

Lawrence Livermore National Laboratory
P.O. Box 808
Livermore, CA 94550
Attn:
Tech. Info. Dept. L-3 1 copy
D.J. Meeker 1 copy
R.E. Batzel/J. Kahn,L-1 1 copy
J.L. Emmett, L-488 1 copy
E. Storm, L-481 1 copy
W.F. Krupke, L-488 1 copy
J. Lindl, L-477 1 copy

Los Alamos National Laboratory
P.O. Box 1663
Los Alamos, NM 87545
Attn: M. Gillispie/Theo.Div. 1 copy
S.D. Rockwood,ICF Prog. Mgr.
DAD/IF M/S 527 6 copies

Massachusetts Institute of Technology
Cambridge, MA 02139
Attn: R.C. Davidson 1 copy
G. Bekefi 1 copy

Maxwell Laboratories, Inc.
9244 Balboa Avenue
San Diego, CA 92123
Attn: J. Pearlman 1 copy

Mission Research Corporation
1400 San Mateo Blvd. SE
Albuquerque, NM 87108
Attn: B.B. Godfrey 1 copy

National Science Foundation
Mail Stop 19
Washington, DC 20550
Attn: D. Berley 1 copy

Naval Research Laboratory
Addressee: Attn: Name/Code
Code 2628 -TID Distribution 20 copies
Code 1001 - T. Coffey 1 copy
Code 4000 - W. Ellis 1 copy
Code 4040 - J. Boris 1 copy
Code 4700 - S.L. Ossakow 26 copies
Code 4701 - I.V.Vitkovitsky 1 copy
Code 4704 - C. Kapetanakos 1 copy
Code 4720 - J. Davis 1 copy
Code 4730 - S. Bodner 1 copy
Code 4740 - W. Manheimer 1 copy
Code 4760 - B. Robson 1 copy
Code 4770 - G. Cooperstein 10 copies
Code 4770.1 - F. C. Young 1 copy
Code 4773 - R.A. Meger 1 copy
Code 4773 - S.J. Stephanakis 1 copy
Code 4790 - D. Colombant 1 copy
Code 4790 - I. Haber 1 copy
Code 4790 - M. Lampe 1 copy
Code 6682 - D. Nagel 1 copy

Physics International Co.
2700 Merced Street
San Leandro, CA 94577
Attn: A.J. Toepfer 1 copy

Pulse Sciences, Inc.
1615 Broadway, Suite 610
Oakland, CA 94612
Attn: S. Putnam 1 copy

R&D Associates
Suite 500
1401 Wilson Blvd.
Arlington, VA 22209
Attn: P.J. Turchi 1 copy

SAI
8400 W. Park Ave.
McLean, VA 22102
Attn: A. Drobot 1 copy

R&D Associates
P.O. Box 9695
Marina Del Rey, CA 90291
Attn: C. MacDonald 1 copy

Sandia National Laboratories
P.O. Box 5800
Albuquerque, NM 87185
Attn: P.Vandevender/1200 6 copies

Spire Corporation
P.O. Box D
Bedford, MA 01730
Attn: R.G. Little 1 copy

Stanford University
SLAC
P.O. Box 4349
Stanford, CA 94305
Attn: W.B. Herrmannsfeldt 1 copy

University of California
Irvine, CA 92717
Attn: N. Rostoker 1 copy

University of Rochester
250 East River Road
Rochester, NY 14623
Attn: J. Eastman 1 copy

Univ. of Washington
Dept. of Nuclear Engineering
BF-10
Seattle, WA 98115
Attn: F. Ribe 1 copy

Director of Research
U.S. Naval Academy
Annapolis, MD 2 copies

DEPARTMENT OF THE NAVY

NAVAL RESEARCH LABORATORY
Washington, D.C. 20375-5000

OFFICIAL BUSINESS
PENALTY FOR PRIVATE USE, $300

POSTAGE AND FEES PAID
DEPARTMENT OF THE NAVY
DoD-316
THIRD CLASS MAIL

END

FILMED

7-85

DTIC